Synthesis and Characterization of Novel Thienothiadiazole-Based D−π−A−π−D Fluorophores as Potential NIR Imaging Agents

Nicholas E. Sparks, Sajith M. Vijayan, Juganta K. Roy, Austin Dorris, Ethan Lambert, Dilan Karunathilaka, Nathan I. Hammer, Jerzy Leszczynski, and Davita L. Watkins*

Read Online

ACCESS | Metrics & More | Article Recommendations | Supporting Information

ABSTRACT: As fluorescence bioimaging has increased in popularity, there have been numerous reports on designing organic fluorophores with desirable properties amenable to perform this task, specifically fluorophores with emission in the near-infrared II (NIR-II) region. One such strategy is to utilize the donor−π−acceptor−π−donor approach (D−π−A−π−D), as this allows for control of the photophysical properties of the resulting fluorophores through modulation of the highest occupied molecular orbital (HOMO) and the lowest unoccupied molecular orbital (LUMO) energy levels. Herein, we illustrate the properties of thienothiadiazole (TTD) as an effective acceptor moiety in the design of NIR emissive fluorophores. TTD is a well-known electron-deficient species, but its use as an acceptor in D−π−A−π−D systems has not been extensively studied. We employed TTD as an acceptor unit in a series of two fluorophores and characterized the photophysical properties through experimental and computational studies. Both fluorophores exhibited emission maxima in the NIR-I that extends into the NIR-II. We also utilized electron paramagnetic resonance (EPR) spectroscopy to rationalize differences in the measured quantum yield values and demonstrated, to our knowledge, the first experimental evidence of radical species on a TTD-based small-molecule fluorophore. Encapsulation of the fluorophores using a surfactant formed polymeric nanoparticles, which were studied by photophysical and morphological techniques. The results of this work illustrate the potential of TTD as an acceptor in the design of NIR-II emissive fluorophores for fluorescence bioimaging applications.
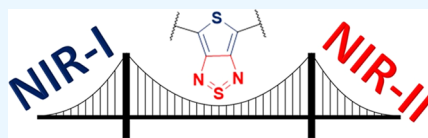
INTRODUCTION

Fluorescence imaging (FI) using near-infrared (NIR) emissive materials is an important and heavily researched area in chemistry due to being a noninvasive technique that has grown in popularity to monitor *in vitro* and *in vivo* physiological processes.[1−3] Among the many materials that have been studied, small-molecule organic dyes are promising candidates due to their tunability and decreased cytotoxicity.[4,5] Strategic design principles are employed to alter the optical properties of organic dyes, which enables a wide range of structural motifs to be synthesized. To that extent, only a handful of small-molecule organic fluorophores are FDA-approved for *in vivo* FI, *i.e.*, indocyanine green (ICG) and methylene blue (MB).[6] Although ICG and MB have optical properties that enable their use in FI applications, they suffer from drawbacks due to their NIR-I (700−1000 nm) emissive properties. NIR-I emissive dyes are primarily known to have issues with *in vivo* applications due to the backscattering of emitted photons along with the autofluorescence of human tissues.[7,8] In addition, NIR-I emissive fluorophores generally require excitation with higher energy light sources which can disrupt cellular functions.[9] The aforementioned issues can be alleviated by employing dyes that emit in the NIR-II region (1000−1700 nm).

In this work, two dyes were synthesized based on the donor−π−acceptor−π−donor approach (D−π−A−π−D)

with emission maxima extending to the NIR-II region. The D−π−A−π−D motif has been utilized in numerous publications, resulting in fluorophores with varying optical properties.[10,11] The D−π−A−π−D design strategy allows for control of the energy gap between the highest occupied molecular orbital (HOMO) and the lowest unoccupied molecular orbital (LUMO), as control of the energy gap is crucial to obtain fluorophores with the desired optical properties. The HOMO resides on the electron-rich donor unit while the LUMO is found on the electron-poor acceptor unit and by varying the strength of the donor and acceptor units. The π-spacer facilitates charge transfer between the acceptor and donor units and can also act as an auxiliary donor. This intramolecular charge transfer (ICT) can result in fluorophores with small energy gaps correlating to lower energy electronic transitions. The D−π−A−π−D strategy can also be used in conjunction with the extension of the π-conjugation of the fluorophore to induce bathochromic shifts of the optical properties. Elongation of the π-conjugated

R=
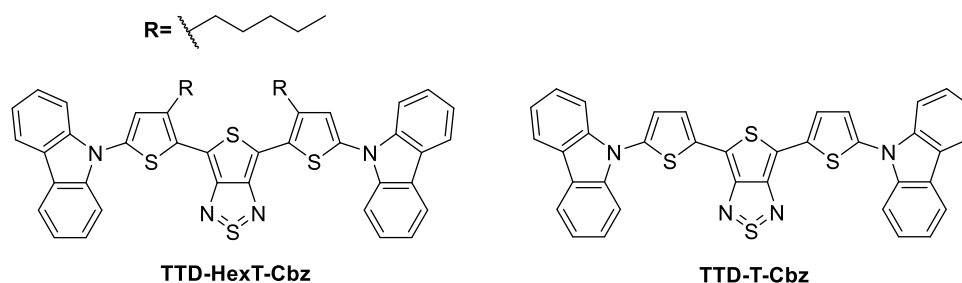
Figure 1. Structures of the two target compounds: **TTD-HexT-Cbz** and **TTD-T-Cbz**.

system typically results in fluorescence quenching through intermolecular interactions, such as $\pi-\pi$ stacking, which must be considered when designing emissive fluorophores.[12]

Previous work in our group utilized isoindigo as the electron-poor acceptor unit, but the optical properties of those dyes were limited with regard to FI applications.[13] Isoindigo, as an acceptor, faces several structural and electronic hurdles that limit its ability to achieve NIR-II emission.[14,15] Our next approach toward designing NIR-II emissive fluorophores was to employ a more electron-deficient acceptor unit, and for this work, we chose thienothiadiazole (TTD). The first report of a TTD-based derivative was in 1969 by Bower et al., and since then, researchers have attempted to harness the electronic properties of the nonclassical bicyclic acceptor.[16−18] When TTD is employed in π-conjugated systems, the quinoidal form tends to be favored upon excitation, which positively affects the optical properties of the system.[18] Further manipulation of the electronic structure of the TTD-based fluorophore by using donor units in addition to the preferred pro-quinoidal structure will result in NIR-I emissive fluorophores with emission extending to the NIR-II.

Carbazole (Cbz) is a well-known electron donor unit used widely in the literature to produce compounds with tunable optical properties. Additionally, it is cost-effective and can be modified with relative synthetic ease, making it a viable option for use.[19] Two different thiophene derivatives were used to create the two fluorophores: one functionalized with an alkyl chain at the 4-position (HexT) and one without an alkyl chain (T). The use of thiophene as a heterocyclic spacer in D−π−A−π−D fluorophores is well reported due to enhanced photostability and ICT character.[20,21] The variation in the thiophene spacer was performed to measure the effects of the alkyl chains on the ground- and excited-state geometries and the subsequent effects on the optical properties of the fluorophores.[22]

Herein, we discuss the theoretical and experimental studies and the subsequent results for the novel TTD-based D−π−A−π−D fluorophores: **TTD-HexT-Cbz** and **TTD-T-Cbz** (Figure 1). Few reports detail TTD-based small-molecule fluorophores, which allows our work to shed important light on the future design and synthesis of other D−π−A−π−D type small-molecule fluorophores that utilize TTD as an acceptor.[23] The two derivatives were studied through computational and experimental methods to understand the optical and structural properties. The two fluorophores exhibited NIR-I emission, extending into the NIR-II region with relative quantum yield (QY) values similar to those observed with other NIR-I emissive fluorophores.[24]

Encapsulation is necessary to study the hydrophobic fluorophores in aqueous environments. We utilized Pluronic-F127, a commercially available and well-studied surfactant commonly used in biomedical applications.[25] The fluorophores were loaded into Pluronic-F127-based self-assembled aggregates to yield fluorescent nanoparticles, to which the nanoparticle solutions were characterized through optical and particle size techniques. Observed shifts of the optical properties were seen upon aggregation in the nanoparticle environment. The experimental results for both the free and encapsulated fluorophores will provide insight into designing TTD-based fluorophores with enhanced optical properties for FI applications.

■ EXPERIMENTAL SECTION

Materials. Reagents and solvents were purchased from commercial sources and were used without further purification. Anhydrous solvents were obtained from a Glass Contour (Irvine, CA) solvent system. Thin-layer chromatography was performed using SiO_2-60 F254 aluminum plates with visualization by ultraviolet (UV) light. Flash column chromatography was performed using a Purasil SiO_2-60, 230−400 mesh from Whatman.

Instrumentation. Nuclear magnetic resonance (NMR) spectra were obtained on a Bruker (Milton, ON, Canada) 400 MHz spectrometer with the appropriate deuterated solvents. Mass spectrometry of the target compounds (0.1 mg/mL) was performed on a Bruker (Milton, ON, Canada) Elute SP HPLC with Bruker Impact II QqTOF Mass Spectrometer under electrospray ionization (ESI) conditions. Electron paramagnetic resonance (EPR) spectroscopy was performed with a Bruker (Milton, ON, Canada) Magnettech ESR5000 spectrometer with 1 mM solutions ($CDCl_3$) of each fluorophore. Quantification of spin states was calculated using $Cu(II)(OTf)_2$ in 1 mM THF. Absorption measurements were carried out on a Varian Cary-500 spectrometer (Dorval, OC, Canada) in dichloromethane (DCM).

Emission spectra were acquired with the Horiba LabRAM HR Evolution Raman Spectroscopy system (Horiba Scientific, Kyoto, Japan) equipped with a 600 grooves/mm grating and charge-coupled device (CCD) detector (Horiba Synapse Silicon CCD, Kyoto, Japan). A 633 nm diode laser (Melles Griot, Takigawa, Hokkaido, Japan) was used as the excitation source. Fluorescence quantum yields (FQY) were measured with samples at 1×10^{-4} M in DCM and relative to IR820 in methanol with an FQY of 4.4%. The spectroscopic energy gap (E_g^{opt}) was calculated from the onset of the absorbance peak maxima.[26] The overall uncertainty for optical experimental values is ±1 nm (0.01 eV).

Fluorescence lifetimes (τ_{FL}) were obtained using the 650 nm output of an LDH series 650P pulsed diode laser as the excitation source (200 μW) and a PicoQuant PDM series single-photon avalanche diode (time resolution approx. 50 ps) as the detector with a Nikon Eclipse TE2000-U microscope. A

TimeHarp 260 time-correlated single-photon counter (25 ps resolution) was used to analyze the photons, as reported previously.[27] Lifetimes were acquired in DCM at a concentration of 1×10^{-4} M. The total instrument response function of the setup was determined to be approx. 200 ps. Fluorescence kinetics were fit with a single-exponential decay function eq 1.

$$I(t) = I(0)e^{-(x-x_0)/\tau_{FL}} \qquad (1)$$

where $I(0)$ represents the initial fluorescence intensity and τ_{FL} represents the fluorescence lifetime.

Time-resolved absorption studies were implemented to acquire excited-state dynamic information. A 1 kHz regeneratively amplified Ti/Sapphire laser (Coherent Astrella, Santa Clara, California) with a 7 W, 100 fs output pulse centered at 800 nm was split with an 85−15 beamsplitter to generate pump and probe beams. To generate the pump, the reflected portion of the 800 nm output was directed into a commercial optical parametric amplifier (OPerA Solo, Vilnius, Lithuania) to generate a 650 nm pump beam. Both the output of the OPerA Solo as well as the remainder of the originally transmitted 800 nm light were directed into commercial transient absorption spectrometers (Ultrafast Systems Helios and Eos, Sarasota, Florida). The pump pulse was chopped at 500 Hz before depolarizing and focused with a 350 mm focal length lens to the sample position. For ultrafast measurements, the remaining 800 nm light was first passed onto a mechanical delay stage before being focused onto a translating CaF_2 crystal to generate a visible white light continuum from 425 to 850 nm. The white light was then filtered to remove any remaining fundamental light and split into probe and reference beams. The reference beam is then reflected into a separate camera to account for jitter and intensity fluctuations. Ultrafast data for each sample were collected by averaging 3 scans with 2 s of averaging at each time delay and corrected with a polynomial to account for temporal chirp. Samples were held in 2 mm quarts cuvettes (FireflySci, Inc., Staten Island, New York). Single-wavelength kinetics were fit with a biexponential decay function eq 2 fit with a biexponential decay function

$$\Delta OD(t) = A_1e^{-(x-x_0)/\tau_1} + A_2e^{-(x-x_0)/\tau_2} \qquad (2)$$

where A_1 and A_2 represent the weights of lifetimes τ_1 and τ_2, respectively. From these lifetime values, an average lifetime τ_{avg} was calculated by eq 3.

$$\tau_{avg} = \frac{A_1\tau_1 + A_2\tau_2}{A_1 + A_2} \qquad (3)$$

Nanoparticles were formed utilizing a thin-film nanoparticle formation technique. Particle size and polydispersity index (PDI) were measured utilizing a Malvern Instrument Zetasizer Nano ZS using a 633 nm wavelength He−Ne laser with a detector angle of 173° at 25 °C. Standard transmission electron microscopy (TEM) was used for the Pluronic-F127 encapsulated dyes. For standard TEM, carbon coated 300 mesh grids were plasma cleaned before applying the nanoparticle solution. The grids were then imaged using a JEOL 1230 TEM with a 100 kV accelerating voltage.

Computational Details. To explore the ground-state geometric and electronic structures of the two derivatives, density functional theory (DFT)-based calculations were performed. Ground-state (S_0) geometry and frequency calculations were computed at DFT/B3LYP/6-31G(d,p)

level of theory. Harmonic vibrational frequencies are computed to confirm that all of the stationary points on the potential energy surface are in minimum energy. The vertical singlet excitation energies are estimated at their ground-state optimized geometries by considering the 10 lowest-lying singlet excited states in the gas phase to simulate the UV−visible (UV−vis) absorption spectra within the conventional time-dependent density functional theory (TD-DFT) formalism. ωB97XD refers to a modified B97 exchange−correlation (XC) functional and incorporates the long-range correction deploying the atom-atom dispersion. To confirm the experimental absorption profile TD-DFT calculations were performed at ωB97XD/6-31G(d,p) level of theory.[28] Full TD-DFT optimizations of the first excited state (S_1) were performed by the ωB97XD/6-31G(d,p) level of theory, and the optimized geometry was used to simulate emission spectra of S_1 state. All of the calculations were carried out using the Gaussian 16 package.[29]

■ RESULTS

Design and Synthesis. The two title compounds were designed and synthesized to obtain NIR-II emissive small-molecule fluorophores. Previous work in our group has resulted in fluorophores with emission maxima in the NIR-I.[13] NIR-I emissive fluorophores have been used for FI applications but suffer from issues such as low penetration depth and increased backscattering of emitted photons *in vivo*.[7,8] NIR-II emissive fluorophores have been shown to alleviate these issues; conversely, in this work, multiple concepts are utilized to design NIR-II emissive fluorophores.[30] First is using the D−π−A−π−D molecular architecture, a well-known design strategy in the literature that has resulted in fluorophores with distinct optical properties.[31] The second concept is to design the fluorophores with the goal of increasing their ICT properties.[32] Efficient ICT can occur due to the localization of the HOMO on the donor unit and the LUMO on the acceptor moiety. Designing fluorophores with a clearly defined and localized HOMO on the donor moiety is difficult as delocalization of the HOMO occurs along the backbone of the fluorophore.[33] There are acceptor moieties that show increased localization of the LUMO.[33] Combining these concepts should allow us to design NIR-II emissive fluorophores with desirable properties, such as high quantum yield and molar absorptivity values.

We utilized the TTD acceptor with varying donor units to create two novel fluorophores. The TTD acceptor is well known for its use in material applications as it is frequently applied as an acceptor in polymeric materials.[33,34] However, only recently has its properties as an acceptor in small molecules been exploited for use in NIR-II FI.[23] The optical properties of previously synthesized TTD-based dyes have been attributed to ICT, but there is evidence that TTD-based dyes can also possess biradicaloid (BRC) species. The presence of BRC species is known to reduce the HOMO−LUMO gap in organic fluorophores, although, upon relaxation, these species are known to be nonemissive. However, through the use of TTD and an appropriate donor unit, we expect to obtain fluorophores with emission maxima approaching the NIR-II region.[35]

The electron-rich donor employed in these two fluorophores is carbazole (Cbz). Aryl amine donors are frequently used in the design and synthesis of D−π−A−π−D fluorophores as they can impart varying properties dependent upon the

intended use of the emissive species.[36] The overall stability of the fluorophore is shown to increase by utilizing aryl amine donors.[37,38] Analysis of theoretical ionization potentials (IP) has shown that Cbz is a moderate electron donor, while structurally, the carbazole moiety is known to have a larger dihedral angle between itself and the π-spacer that is being used.[37,39] This can assist in reducing aggregation and prevent fluorescence quenching of the fluorophore. The large dihedral angle can also effectively have a clearly defined HOMO residing on the Cbz donor, which should assist in the ICT nature of the fluorophores.[39] Considering the aforementioned characteristics of Cbz and in conjunction with synthetic accessibility, we chose to utilize it as our electron donor.

Thiophene is utilized as the π-spacer in this work as it is a commonly used heterocycle in the design of D−π−A−π−D emissive fluorophores.[40] Thiophene exhibits a lower degree of aromaticity and directly correlates to its ability to take on a quinoidal form upon excitation, decreasing the overall HOMO−LUMO gap and allowing for lower energy electronic transitions to occur.[41,42] Two derivatives of thiophene are used in this work, one that possesses a hexyl chain at the 4-position of the thiophene (**TTD-HexT-Cbz**), and one that does not (**TTD-T-Cbz**).[43] The alkyl chain aids in increasing the solubility of the fluorophore in organic solvents. Additionally, we can evaluate their effect on the structural conformations of the fluorophore due to their proximity to the acceptor core. The alkyl chain can act as a shielding unit to protect the TTD acceptor from incoming solvent molecules. This protection results in the enhancement of the fluorophore's optical properties, such as the fluorescent quantum yield (QY), by reducing nonradiative energy loss from the excited-state species to the solvent.[44] The thiophene that lacks the alkyl chain (i.e., **TTD-T-Cbz**) will allow the derivative to obtain a more planar conformation with respect to the flanking thiophenes and the TTD acceptor.[45] This increases planarity affording enhanced ICT upon excitation.

The donor units, HexT-Cbz and T-Cbz, were synthesized using modified Ullmann conditions, resulting in yields of 29 and 32%, respectively. Stannylation of the HexT-Cbz and T-Cbz donor units was performed to couple the donor units to 2,5-dibromo-3,4-dinitrothiophene under Stille conditions. Intermediates **7** and **8** were obtained in yields of 41 and 23% and then reduced accordingly using a previously reported procedure to the corresponding amines **9** and **10** with 27 and 37% yields, respectively.[44] The target compounds **TTD-HexT-CBz** and **TTD-T-Cbz** were obtained after intermediates **9** and **10** underwent cyclization, using the reported procedure, in yields of 45 and 2% (Figure 1 and Scheme S1).[44] The title compounds were both observed to be greenish-blue powder in the solid state and, upon solvation in organic solvents, were seen to produce a teal-colored solution. The full synthetic scheme and ^{1}H NMR and ^{13}C NMR spectra can be found in the Supporting Information, Scheme S1 and Figures S1−S10.

Computational Correlations. In order to estimate the energetics of the ground-state frontier molecular orbitals (FMOs) of **TTD-HexT-Cbz** and **TTD-T-Cbz** and their corresponding HOMO−LUMO gaps (E_{gap}^{HL}), the B3LYP/6-31G(d,p) level of theory was employed. Experimentally, the **TTD-T-Cbz** and **TTD-HexT-Cbz** derivatives possess optical bandgaps (E_{gap}^{opt}) of 1.91 and 1.94 eV, respectively, which we then compare with the theoretical E_{gap}^{HL}. The computed E_{gap}^{HL} for the two derivatives was found to be 1.76 eV for **TTD-T-Cbz** and 1.92 eV for **TTD-HexT-Cbz**. There is a noticeable

difference between the theoretical and experimental band gap values for the **TTD-T-Cbz** and can be explained by **TTD-T-Cbz's** planar structure in both the ground (S_0) and excited (S_1) states. Most notably, the bond angle (φ_2) shows only a change of 1.79° between S_0 and S_1 for **TTD-T-Cbz**, while the difference in that same bond angle is 16.7° for **TTD-HexT-Cbz**. Correlating this to the computed E_{gap}^{HL} for **TTD-T-Cbz**, the increased planarity would result in a decrease in the HOMO−LUMO gap for **TTD-T-Cbz**.[46] In addition, as the computational E_{gap}^{HL} values were obtained in the gas phase, intermolecular and solvent interactions were not considered. Considering these aspects, the deviation between the experimental and computational HOMO−LUMO gap values is understandable. The increased planarity of the **TTD-T-Cbz** derivative can allow for π−π stacking interactions, which appear to have a negative impact on the emissive properties of the **TTD-T-Cbz** derivative. We also observe the importance of the hexyl chains on the thiophene spacer unit, as they appear to play an important role in the photophysical properties of the two derivatives. As **TTD-T-Cbz** lacks the hexyl chains, the TTD core is prone to be solvated by solvent molecules which can affect the optical properties of the dye.

The frontier molecular orbitals (FMO) isoelectronic density distribution for the two derivatives can be seen in Figure 2. For
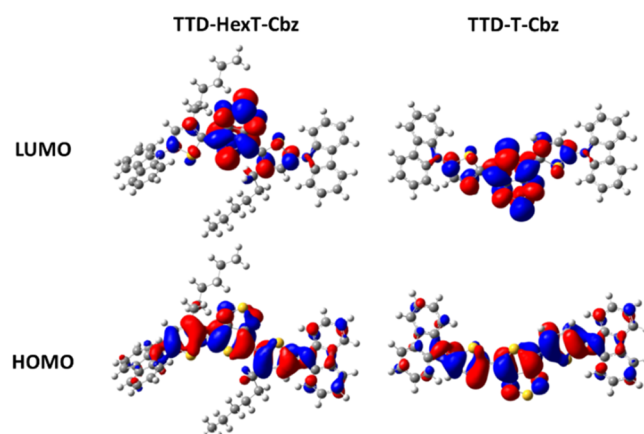
Figure 2. Ground-state HOMO−LUMO gap (E_{gap}^{HL}) and vertical excitation energy ($E_{0\rightarrow 1}^{vert}$) along with FMOs density map (isovalue 0.02 au) of the TTD derivatives at the level of theory in the gas phase.

both derivatives, the corresponding HOMOs were observed to be distributed along the conjugated backbone. This is commonly observed with D−π−A−π−D fluorophores, as localization of the HOMO on the donor unit is difficult.[33] We do see increased localization of the LUMOs on the TTD acceptor moieties, with some delocalization onto the thiophene spacer units. For **TTD-T-Cbz**, the LUMO extends further onto the thiophene spacers, resulting from the increased planarity of the derivative. The LUMO of the **TTD-HexT-Cbz** derivative is primarily localized on the TTD acceptor and is another indication of the importance of the hexyl chains on the thiophene spacer and the role it plays in modulating the photophysical properties of the **TTD-HexT-Cbz** derivative. For both derivatives, the major electronic transition is associated with the HOMO and the LUMO, as these transitions possess the highest oscillator frequency value. The S_0 to S_n transition data for all transitions (oscillator strength >0.1) can be found in the Supporting Information, Table S1.

Table 1. DFT/TD-DFT Computed Dihedral Angles of TTD-HexT-Cbz and TTD-T-Cbz
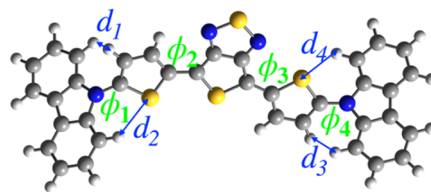
	φ_1	φ_2	φ_3	φ_4	$\mu_{S_0}|\mu_{S_1}$	d_1	d_2	d_3	d_4
	$S_0|S_1$	$S_0|S_1$	$S_0|S_1$	$S_0|S_1$	debye	$S_0|S_1$	$S_0|S_1$	$S_0|S_1$	$S_0|S_1$
TTD-HexT-Cbz	115.60|125.55	139.19|155.86	177.49|178.65	120.99|131.45	1.40|1.39	1.40|1.39	1.43|1.41	1.43|1.41	1.40|1.40
TTD-T-Cbz	118.85|129.56	177.29|179.50	177.37|179.50	118.85|129.56	2.75|2.42	2.75|2.42	3.06|2.84	2.75|2.48	3.02|2.84

To identify the biradical character of two studied TTD derivatives qualitatively, the singlet−triplet energy gap (ST_{gap}) was computed and the values are 0.416 and 0.528 eV for **TTD-T-Cbz** and **TTD-HexT-Cbz**, respectively. To compute ST_{gap}, zero-point energy (ZPE) corrected values were considered, which is called adiabatic ST_{gap}. Following Wirz, a molecule is biradicaloid when the adiabatic ST_{gap} is between 0.01 and 1.0 eV (2−24 kcal mol^{-1}). In turn, it would not be an exaggeration to claim that these molecules are indeed biradicaloids.[46] However, the lowest value corresponds to **TTD-T-Cbz** (0.416 eV).

Computed bond lengths and dihedral angles of ground- and first excited-state dipole moments can be found in Table 1 (the optimized geometry of ground and first excited states are given in Supporting Information, Figures S11 and S12). It is seen that the ground-state dipole moments for both derivatives are more significant than the excited-state dipole moments, as there is an increase in planarity for both derivatives upon excitation. **TTD-T-Cbz** and **TTD-HexT-Cbz** have a large perturbation in the C−N−C−S dihedral angles (φ_1 and φ_4) and between the flanking carbazole donor units and the thiophene spacers, but upon excitation, there is an increase in planarity. Through analysis of the S−C−C−C bond angles (φ_2 and φ_3) for **TTD-T-Cbz**, we can see that the thiophene spacer is essentially coplanar with the TTD acceptor in both the ground and excited states. Looking at the same dihedral angles for **TTD-HexT-Cbz**, there is an increased perturbation, which underlines the effect the hexyl chain has on the structure. The φ_2 dihedral angle is quite large, which underlines the effect the hexyl chain has on the structure.

Interestingly, the φ_3 dihedral angle is much smaller in comparison to φ_2, indicating planarity with the TTD acceptor. Upon excitation, however, we do observe an increase in planarity for the φ_2 dihedral angle while the φ_3 dihedral angle does not change much as it is essentially planar in the ground and excited states.

Spectroscopic Analysis. UV−vis−NIR absorption and emission studies were performed to investigate the optical properties of the two derivatives. Solutions (8 × 10^{-5} M DCM) of both derivatives were made and analyzed using UV−vis−NIR absorbance spectroscopy. **TTD-HexT-Cbz** possessed an λ_{max}^{abs} = 638 nm with an λ_{onset}^{abs} = 824 nm, while **TTD-T-Cbz** was observed to have an λ_{max}^{abs} = 651 nm and λ_{onset}^{abs} = 796 nm (Figure 3).[47] The trend in the λ_{max}^{abs} data for the two derivatives correlates with what is observed in the computational data. The experimental molar absorption coefficients (ε) were obtained by taking the absorptivity value at λ_{max}^{abs} and were calculated to be 2.3 × 10^4 M^{-1} cm^{-1} for **TTD-T-Cbz** and 4.2 × 10^4 M^{-1} cm^{-1} for **TTD-HexT-Cbz**. The computed oscillator
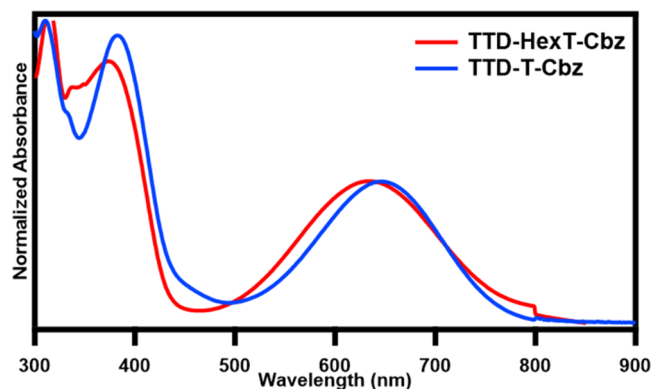

Figure 3. Normalized UV−vis−NIR absorbance spectra of **TTD-HexT-Cbz** (red) and **TTD-T-Cbz** (blue) in 8 × 10^{-5} M DCM.
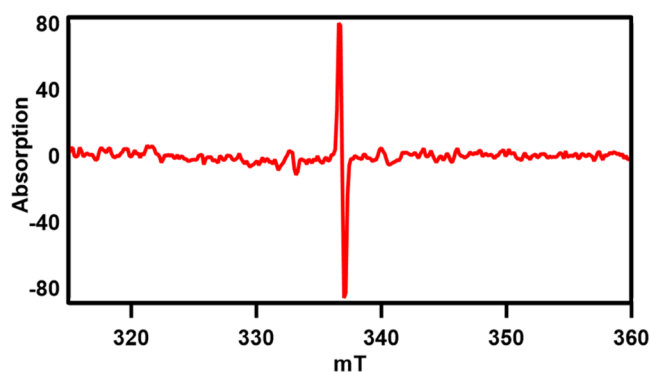
strengths do not correlate to the experimental molar absorption coefficients as **TTD-T-Cbz** (f = 0.569) is predicted to be more efficient at absorbing radiation than **TTD-HexT-Cbz** (f = 0.493). Theoretical absorbance and emission spectra can be found in the Supporting Information, Figure S13. Tabulated experimental and theoretical photophysical data can be seen in Table 2.

The two derivatives exhibited emission into the further reaches of the NIR-I region, with peak maxima of 891 and 900 nm for **TTD-T-Cbz** and **TTD-HexT-Cbz**, respectively. Interestingly, the emission onsets were found to extend into the NIR-II region past 1000 nm, which is past the detection limit of the spectrometer used (Figure 4). The trend observed in the theoretical λ_{max}^{emi} matches what is observed experimentally, but the values for the λ_{max}^{emi} do not correlate well between the experimental and theoretical values. This can be attributed to the fact that it is more difficult to predict, through computational methods, properties that are affected by the LUMO such as fluorescence.[48] Experimental relative quantum yields (QY, Φ) were found to be 0.30 and 0.48% for **TTD-T-Cbz** and **TTD-HexT-Cbz**. Once again, the structural differences between the two derivatives are seen to affect the optical properties of the dyes. Fluorescent lifetime values (τ_{FL}) were measured to be 204.7 and 195.2 ps for **TTD-T-Cbz** and **TTD-HexT-Cbz**. Fluorescence lifetime curves for the two derivatives can be found in the Supporting Information, Figures S14 and S15.

Electron paramagnetic resonance (EPR) spectroscopy was utilized to rationalize the differences in QY between the two derivatives. **TTD-T-Cbz** exhibited a large signal at 336 mT (g = 2.006) that is indicative of one unpaired electron (Figure 5). We determined the concentration of spin states for **TTD-T-**

Table 2. Experimental (8×10^{-5} M DCM) and Theoretical Spectroscopic Data of TTD-T-Cbz and TTD-HexT-Cbz

	experimental						theoretical			
	λ_{max}^{abs} (nm)	λ_{max}^{emi} (nm)	Stokes shift [nm (cm^{-1})]	ε ($\times 10^4$ M^{-1} cm^{-1})	τ_{FL} (ps)	QY (%)	λ_{max}^{abs} [nm (eV)]	λ_{max}^{emi} [nm (eV)]	Stokes shift [nm (cm^{-1})]	f $S_0(S_1)$
TTD-T-Cbz	651	891	240 (4.16×10^4)	2.3	204.76	0.30	663 (1.87)	841 (1.47)	179 (5.58×10^4)	0.569 (0.471)
TTD-HexT-Cbz	638	900	262 (3.81×10^4)	4.2	195.24	0.48	622 (1.99)	815 (1.52)	194 (5.15×10^4)	0.493 (0.424)
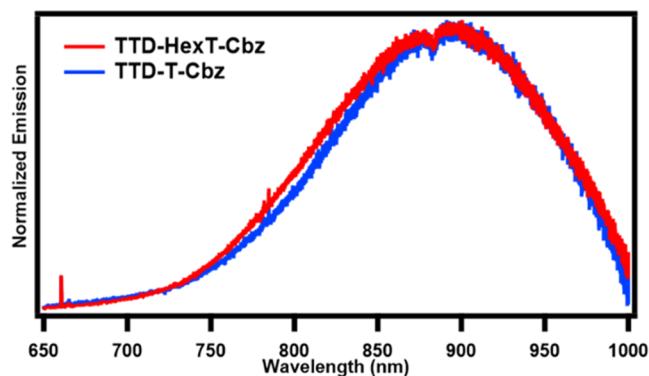
Figure 4. Normalized NIR emission spectra of **TTD-HexT-Cbz** (red) and **TTD-T-Cbz** (blue) in 8×10^{-5} M DCM.

Figure 5. EPR spectrum of **TTD-T-Cbz** in 1 mM CDCl$_3$.

Figure 6. UV−vis−NIR absorbance spectra of 1 mg/mL solutions of **TTD-HexT-Cbz** NPs (red) and **TTD-T-Cbz** NPs (blue).

Cbz to be 138 μM (13.8%) in the 1 mM sample. To our knowledge, this is the first experimental example of a TTD-based small molecule possessing radicals. **TTD-HexT-Cbz** did not show any appreciable signal due to the hexyl groups distorting the conjugated backbone of the fluorophore. The structural distortion is a destabilizing effect that prevents the formation of an unpaired electron as the ability to delocalize is removed, unlike **TTD-T-Cbz**, which is more planar. EPR spectra for **TTD-HexT-Cbz** can be found in the Supporting Information, Figure S16.

Encapsulation of the two derivatives into Pluronic-F127 surfactant and studying the optical properties of the nanoparticle solutions provide information as to how these fluorophores act in an aggregated environment. Encapsulation of fluorophores into a nanoaggregate can affect the optical properties of the fluorophore, so it is necessary to optically characterize the nanoparticle solutions.[49] Nanoparticle solutions were prepared and then studied using the same optical techniques used to study the fluorophores in organic solvents. The encapsulated **TTD-HexT-Cbz** showed a bathochromic shift of its absorbance maxima to 662 nm, while we observed a bathochromic shift to 667 nm for the encapsulated **TTD-T-**

Cbz (Figure 6). The low-energy absorbance band for the encapsulated **TTD-T-Cbz** also broadens significantly com-
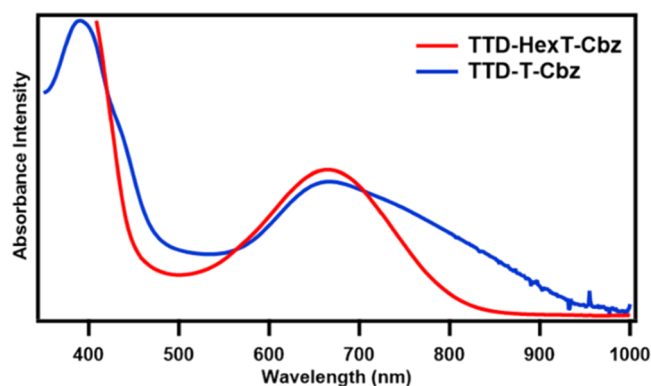
pared to **TTD-T-Cbz** in organic solvent. The emission maxima for the encapsulated **TTD-HexT-Cbz** did not show any notable shift, with an observed λ_{max}^{emi} of 886 nm, but a significant decrease in the relative quantum yield as a value of 0.24% was observed. The emission spectra for the encapsulated **TTD-T-Cbz** show a large broadening of the emissive band with two noticeable shoulders being seen. There is also an observed hypsochromic shift of the emission maxima for the encapsulated **TTD-T-Cbz** (FWHM = 200 nm (5×10^4 cm^{-1})) compared to the free fluorophore (FWHM = 150 nm (6.67×10^4 cm^{-1})) as seen in the normalized emission spectra (Supporting Information, Figure S17). The relative quantum yield for the encapsulated **TTD-T-Cbz** decreased slightly to 0.29%. A bi-modal distribution was observed in the fluorescence lifetime of the encapsulated **TTD-HexT-Cbz** (Supporting Information, Figure S15) as a shorter-lived value of 9.7 ps was seen in addition to a longer-lived value of 360.4 ps. Interestingly, the excited-state lifetimes of the encapsulated **TTD-T-Cbz** were found to be significantly extended, with a value greater than 8 ns being obtained (Supporting Information, Figure S14).

Nanoparticle Morphology Characterization. Nanoparticle solutions of both **TTD-T-Cbz** and **TTD-HexT-Cbz** were formed by thin-film nanoparticle formation techniques using Pluronic-F127 as a surfactant. Micellar-like nanoparticles are formed in aqueous media, with the hydrophobic dyes being internalized into the hydrophobic portion of the Pluronic-F127. Dynamic light scattering (DLS) and TEM were used to characterize nanoparticle morphologies. The average hydrodynamic radius for the **TTD-HexT-Cbz** nanoparticles was found to be 117.8 nm as measured with DLS with a PDI value of 0.310, indicating high polydispersity. Through TEM analysis of the **TTD-HexT-Cbz** nanoparticles, we observed average nanoparticle sizes of 68.3 nm. The **TTD-T-Cbz** nanoparticles
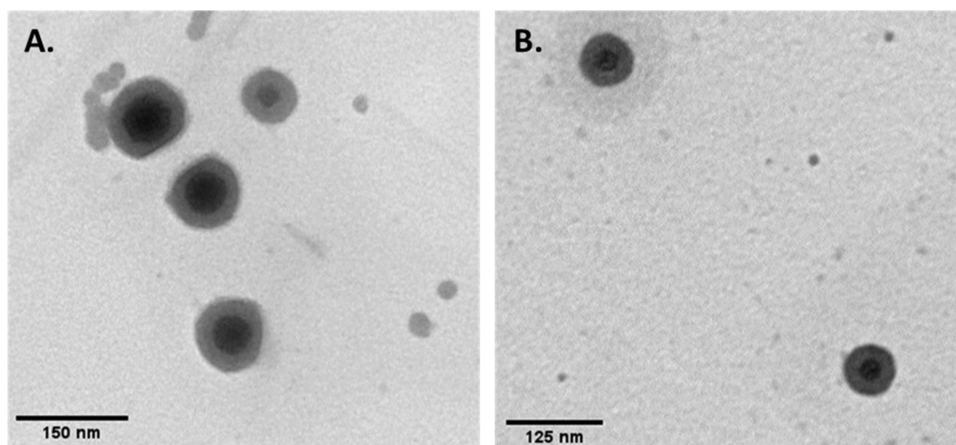
Figure 7. TEM images of **TTD-T-Cbz** NPs (A) and **TTD-HexT-Cbz** NPs (B) at 39,000× magnification.

possessed a larger average hydrodynamic radius of 195.9 nm but a lower PDI value of 0.226. TEM analysis showed average nanoparticle sizes of 90.8 nm for the **TTD-T-Cbz**. We also calculated encapsulation efficiencies (EE) for the two nanoparticle solutions. The **TTD-T-Cbz** nanoparticle solution possessed an EE of 20.0%, while the **TTD-HexT-Cbz** nanoparticles had an EE of 1.9%. TEM images can be seen in Figure 7, while DLS spectra and tabulated size data can be found in the Supporting Information, Figures S18−S21 and Table S2.

■ DISCUSSION

This work aimed to synthesize two D−π−A−π−D fluorophores that employ TTD as an acceptor. In the design of NIR-II emissive fluorophores, we utilize the D−π−A−π−D motif, and by using different donors and acceptors, we can narrow the HOMO−LUMO gap and subsequently control the photophysical properties. Ideally, the HOMO would be localized on the donor, with the LUMO on the acceptor for efficient ICT. This is difficult to achieve as there is commonly some delocalization of the HOMO across the conjugated framework. With that in mind, we wanted to study an acceptor that has been shown to have a localized LUMO, and subsequently chose to use TTD as an acceptor.

Through computational methods, the LUMOs of the two synthesized fluorophores were found to be predominantly localized on the TTD acceptor, as seen in Figure 2. For both derivatives, the primary $(S_0 \rightarrow S_1)$ electronic transitions (<90%) are between the HOMO and the LUMO and are indicative of ICT. For **TTD-T-Cbz**, two other contributing electronic transitions were observed. The first of which is a high energy transition (3.56 eV) with an f = 0.539 that is associated with the $S_0 \rightarrow S_3$ energy levels and involves electron density reorganization from the HOMO to LUMO + 1 (44.7%) and the HOMO − 2 to LUMO (40.7%). The other is a higher energy transition (0.381 eV) with a much lower oscillator frequency of 0.303. This transition is associated with the $S_0 \rightarrow S_4$ energy levels that also involve electron density reorganization from the HOMO to LUMO + 1 (43.4%) and the HOMO − 2 to LUMO (43.1%). **TTD-HexT-Cbz** is shown to have only one other contributing electronic transition associated with the $S_0 \rightarrow S_3$ energy levels. This high energy transition (3.67 eV) leads to electron density reorganization from the HOMO − 2 to LUMO (39.2%) and the HOMO to LUMO + 1 (36.2%). For both derivatives, the

higher energy conversions indicate π to π* transitions. As such, **TTD-HexT-Cbz** appears to have a more localized LUMO, which may result from the increased steric strain from the HexT spacer. The HOMOs for the two derivatives are found to be delocalized across the conjugated backbone of the fluorophores, predominantly on the thiophene spacers. Thiophene derivatives are shown to be able to contribute significantly to the HOMO energy level, which is what is observed in the case of the two derivatives.[50] For **TTD-T-Cbz**, the carbazole units do seem to contribute more to the HOMO because of the increased planarity of the compound. In contrast, there is contribution from only one of the carbazole units on **TTD-HexT-Cbz** due to the distortion of the conjugated backbone.

Experimental optical HOMO−LUMO gaps (E_{gap}^{opt}) for **TTD-T-Cbz** and **TTD-HexT-Cbz** were found to be 1.91 and 1.94 eV, respectively. Similar values are expected as the electronic backbone of the two fluorophores is constant between the two. The difference is the presence of the hexyl groups on the thiophene spacer for **TTD-HexT-Cbz**, resulting in an increased steric strain which decreases the planarity of the derivative. However, **TTD-T-Cbz** does not have the hexyl groups on the thiophene spacer and the E_{gap}^{opt} is found to be slightly lower owing to the extended conjugation of the fluorophore. Upon comparison of the theoretical E_{gap}^{HL}, we see good agreement for the **TTD-HexT-Cbz** with a theoretical value of 1.92 eV. For **TTD-T-Cbz**, there is a noticeable deviation between the experimental and theoretical values as the theoretical E_{gap}^{HL} was found to be 1.76 eV. The hypothesized difference between the theoretical and experimental values for **TTD-T-Cbz** results from solvation effects on the TTD acceptor.[51]

TTD-T-Cbz possessed an experimental λ_{max}^{abs} of 651 nm with a theoretical λ_{max}^{abs} of 663 nm, while **TTD-HexT-Cbz** has an experimental λ_{max}^{abs} of 638 nm and a theoretical λ_{max}^{abs} of 622 nm. The red-shifted λ_{max}^{abs} for **TTD-T-Cbz** is a direct correlation to the increased planarity of the compound.[52] The higher energy transitions (Figure 3) are primarily a result of the π−π* electronic transitions of the conjugated backbone, and the broad absorbance bands are indicative of ICT as a result of the D−π−A−π−D framework. The experimental molar absorption coefficients indicate that **TTD-HexT-Cbz** is a more efficient absorber of radiation than **TTD-T-Cbz** which contradicts with predicted values. This is another example of the effect that the hexyl groups have on the optical properties of the dyes.[53]

The emission maxima and the shape of the emission band of the two fluorophores were found to be similar, which is to be expected as the conjugated framework is constant between the two. We observed an experimental λ_{max}^{emi} of 891 and 900 nm for **TTD-HexT-Cbz** and **TTD-T-Cbz**, respectively. The emission maxima of the two fluorophores are still in the NIR-I region and not in the hypothesized NIR-II region. One explanation for this is the use of the carbazole donor and its ineffectiveness to contribute electron density. The steric bulk of the carbazole donor unit does not allow for the desired contribution of electron density, resulting in an increase of the HOMO level leading to a decrease in the overall HOMO−LUMO gap.[36] Analyzing the relative QY for the two fluorophores, we observe that **TTD-HexT-Cbz** is more emissive than its nonalkylated counterpart. The difference between the two can also be observed in the non-normalized emission spectra of the two dyes, as the emissive band for **TTD-HexT-Cbz** exhibits a greater intensity than that of **TTD-T-Cbz** (Supporting Information, Figure S22). By distorting the conjugated backbone of **TTD-HexT-Cbz** due to the hexyl groups on the thiophene spacers, there is a reduction in intermolecular interactions which allows for the increased relative QY.[44] Another hypothesis for the lower QY value for **TTD-T-Cbz** is the presence of BRC species. BRCs are known to provide low-energy excitations, although upon relaxation that energy is lost nonradiatively.[35] For TTD-based organic fluorophores, only computational studies have illustrated the existence of these radical species. The presence of these unpaired electrons is hypothesized to exist in order to relieve the strain on the hypervalent sulfur atom ($-N=S=N-$) that comprises the thiadiazole ring in the acceptor.[53] We studied both derivatives with EPR to further rationalize the difference in their QY values (Figures 5 and S16). Although we indicate computationally the presence of biradical species ($S = 0$), the results from the EPR study illustrate the presence of a single unpaired electron ($S > 0$) on **TTD-T-Cbz**. We hypothesize the other unpaired electron is lost to the solvent environment which results in an unpaired electron on **TTD-T-Cbz**. Unpaired electrons on conjugated compounds are known to absorb low-energy radiation, but upon relaxation, the absorbed energy is lost nonradiatively. As such, the presence of unpaired electrons on these fluorophores is detrimental to their emissive properties.[54] For **TTD-T-Cbz**, we detected a large signal at 336 mT ($g = 2.006$), while for **TTD-HexT-Cbz** there was no signal detected. This result correlates to the increased planarity of **TTD-T-Cbz** and its ability to stabilize the radical species through delocalization. The presence of unpaired electrons, along with the previously discussed factors, leads to a lower QY value for **TTD-T-Cbz** compared to its alkylated counterpart. The large Stokes shifts observed result from excited-state geometry reorganization to achieve a more planar excited-state geometry.[55] The short-lived excited-state lifetimes for the two fluorophores can be attributed to the energy gap law, which dictates that nonradiative energy processes at longer wavelengths increase due to vibrational overlaps between the ground and excited states (Supporting Information, Figures S23 and S24).[56,57] This negatively affects the excited-state properties of the two derivatives.

The nanoparticle solutions of the two fluorophores exhibited different optical properties compared to the free fluorophores. Analysis of the UV−vis−NIR absorbance (Figure 6) spectra for the **TTD-HexT-Cbz** nanoparticles shows a red shift of the λ_{max}^{abs} to 662 nm, which can be attributed to the formation of lower-energy aggregates within the nanoparticle.[58] The emission spectra for the **TTD-HexT-Cbz** nanoparticles show that these lower-energy aggregates do not affect the fluorescence properties of **TTD-HexT-Cbz**. Since the λ_{max}^{emi} is only slightly blue-shifted to 886 nm compared to the free fluorophore, the emission observed is from the monomeric form of the fluorophore within the nanoparticle (Supporting Information, Figure S17). This can also account for the decrease in QY as fewer emissive species are present within the aggregated environment.[59] The **TTD-T-Cbz** nanoparticles also showed a red shift of the λ_{max}^{abs} to 667 nm. However, the absorbance band had broadened significantly, with the onset of the absorbance band extending past 900 nm (Figure 6). The broad absorbance band indicates the presence of multiple types of aggregates within the nanoparticle. The fluorescent properties of the **TTD-T-Cbz** nanoparticles are shown to be altered upon aggregation. We can see in the emission spectra that there is not only a blue shift of the emission band but there are now two noticeable features seen (Supporting Information, Figure S17). The two peaks at 799 and 856 nm could indicate that different species are present within the aggregated environment that is emissive. Interestingly, the QY for the **TTD-T-Cbz** nanoparticles was found to be similar to what is observed for the free fluorophore, which could be a correlation to the increased encapsulation efficiency of the **TTD-T-Cbz** nanoparticles compared to the **TTD-HexT-Cbz** nanoparticles as more **TTD-T-Cbz** was found to be encapsulated by the Pluronic-F127. The excited-state lifetimes for the **TTD-HexT-Cbz** and **TTD-T-Cbz** nanoparticles were extended compared to the unencapsulated fluorophores. This is due to the stabilization of the excited-state species within an aggregated environment.[60]

DLS analysis of the encapsulated fluorophores indicates that the two fluorophores aggregate differently upon encapsulation (Supporting Information, Table S2). The **TTD-T-Cbz** nanoparticles gave larger average hydrodynamic radii than the **TTD-HexT-Cbz** nanoparticles. This can be attributed to the difference in the amount of fluorophore encapsulated in the polymer nanoparticle, as illustrated by the large differences in EE values. The PDI value for the **TTD-T-Cbz** nanoparticles is lower than that of the **TTD-HexT-Cbz** nanoparticles. However, both nanoparticle solutions indicate polydispersity. It is understood in the field that TEM provides smaller sizes compared to DLS.[61,62] Analysis of the TEM images for both nanoparticle samples indicates the presence of spherical nanoparticles with contrast variations indicative of dye encapsulation. All sizes were below 150 nm and correlate with the trends observed in DLS.

CONCLUSIONS

Two TTD-based D−π−A−π−D fluorophores have been synthesized and characterized through computational and experimental methods. The overarching goal of the work was to study the use of TTD as an electron acceptor in the design of NIR-II emissive fluorophores for FI applications, as few reports employ it in that role. Modulating the HOMO−LUMO gap by employing donors and acceptors with localized FMOs is a strategy that can facilitate low-energy electronic transitions via an ICT pathway. Analysis of the FMOs for the resulting fluorophores, **TTD-HexT-Cbz** and **TTD-T-Cbz**, showed that for both derivatives, the LUMO was localized on the TTD acceptor with the primary electronic transitions occurring between the S_0 to S_1. The two fluorophores showed

broad absorbance bands ranging from the NIR-I to visible regions with emission maxima in the far reaches of the NIR-I extending into the NIR-II. These low-energy transitions are primarily attributed to the ICT nature of the D−π−A−π−D compounds. Both fluorophores exhibited moderate QY values with excited-state lifetimes of approx. 200 ps. We were able to illustrate the presence of unpaired electrons in the **TTD-T-Cbz** derivative to help account for the difference in QY values when comparing the two fluorophores. This is, to our knowledge, the first experimental evidence of the existence of unpaired electrons in a TTD-based small molecule.

The derivatives were encapsulated into Pluronic-F127 surfactant to induce water solubility, which is necessary for FI applications. The morphological properties of the encapsulated fluorophores were found to be micellar-like nanoparticles with sizes ranging from 100 to 200 nm. Bathochromic shifts in absorbance were observed for both derivatives upon encapsulation, along with hypsochromic shifts in the emission maxima. Overall, QY values decreased for the encapsulated fluorophores, while the excited-state lifetimes were found to increase due to the stabilization of the excited-state species. The results from this work provide design strategies in which TTD can be used as an effective electron acceptor moiety for NIR emissive fluorophores in FI applications.

■ ASSOCIATED CONTENT

ⓈI Supporting Information

The Supporting Information is available free of charge at https://pubs.acs.org/doi/10.1021/acsomega.3c02602.

> Full synthetic details and NMR characterization; computational correlations; fluorescence lifetime spectra; EPR spectra; normalized and non-normalized emission spectra; DLS spectra; and TAS spectra (PDF)

■ AUTHOR INFORMATION

Corresponding Author

Davita L. Watkins − *Department of Chemistry and Biochemistry, University of Mississippi University, Oxford, Mississippi 38677, United States; Department of Chemistry and Biochemistry, The Ohio State University, Columbus, Ohio 43210, United States; William G. Lowrie Department of Chemical and Biomolecular Engineering, The Ohio State University, Columbus, Ohio 43210, United States;* ⓞ orcid.org/0000-0002-0943-7220; Email: watkins.891@osu.edu

Authors

Nicholas E. Sparks − *Department of Chemistry and Biochemistry, University of Mississippi University, Oxford, Mississippi 38677, United States; Department of Chemistry and Biochemistry, The Ohio State University, Columbus, Ohio 43210, United States;* ⓞ orcid.org/0000-0001-9578-3869

Sajith M. Vijayan − *Department of Chemistry and Biochemistry, University of Mississippi University, Oxford, Mississippi 38677, United States*

Juganta K. Roy − *Interdisciplinary Center for Nanotoxicity, Department of Chemistry, Physics and Atmospheric Sciences, Jackson-State University, Jackson, Mississippi 39217, United States;* ⓞ orcid.org/0000-0002-3646-5593

Austin Dorris − *Department of Chemistry and Biochemistry, University of Mississippi University, Oxford, Mississippi 38677, United States*

Ethan Lambert − *Department of Chemistry and Biochemistry, University of Mississippi University, Oxford, Mississippi 38677, United States*

Dilan Karunathilaka − *Department of Chemistry and Biochemistry, University of Mississippi University, Oxford, Mississippi 38677, United States*

Nathan I. Hammer − *Department of Chemistry and Biochemistry, University of Mississippi University, Oxford, Mississippi 38677, United States;* ⓞ orcid.org/0000-0002-6221-2709

Jerzy Leszczynski − *Interdisciplinary Center for Nanotoxicity, Department of Chemistry, Physics and Atmospheric Sciences, Jackson-State University, Jackson, Mississippi 39217, United States*

Complete contact information is available at:
https://pubs.acs.org/10.1021/acsomega.3c02602

Author Contributions

The manuscript was written through contributions of all authors. All authors have given approval to the final version of the manuscript.

Notes

The authors declare no competing financial interest.

■ ACKNOWLEDGMENTS

■ ABBREVIATIONS

FI, fluorescence imaging; NIR, near-infrared; ICG, indocyanine green; MB, methylene blue; D−π−A−π−D, donor−π−acceptor−π−donor approach; HOMO, highest occupied molecular orbital; LUMO, lowest unoccupied molecular orbital; ICT, intramolecular charge transfer; TTD, thienothiadiazole; QY, quantum yield; NMR, nuclear magnetic resonance; ESI, electrospray ionization; EPR, electron paramagnetic resonance; DCM, dichloromethane; DMSO, dimethyl sulfoxide; MeCN, acetonitrile; THF, tetrahydrofuran; MePh, toluene; TEM, transmission electron microscopy; DFT, density functional theory; FMO, frontier molecular orbitals

■ REFERENCES

(1) Gao, M.; Yu, F.; Lv, C.; Choo, J.; Chen, L. Fluorescent Chemical Probes for Accurate Tumor Diagnosis and Targeting Therapy. *Chem. Soc. Rev.* **2017**, *46*, 2237−2271.

(2) van Manen, L.; Handgraaf, H. J. M.; Diana, M.; Dijkstra, J.; Ishizawa, T.; Vahrmeijer, A. L.; Mieog, J. S. D. A Practical Guide for the Use of Indocyanine Green and Methylene Blue in Fluorescence-Guided Abdominal Surgery. *J. Surg. Oncol.* **2018**, *118*, 283−300.

(3) Maulvi, F. A.; Lakdawala, D. H.; Shaikh, A. A.; Desai, A. R.; Choksi, H. H.; Vaidya, R. J.; Ranch, K. M.; Koli, A. R.; Vyas, B. A.; Shah, D. O. In Vitro and in Vivo Evaluation of Novel Implantation

Technology in Hydrogel Contact Lenses for Controlled Drug Delivery. *J. Controlled Release* 2016, 226, 47−56.

(4) Shen, Q.; Wang, S.; Yang, N.-D.; Zhang, C.; Wu, Q.; Yu, C. Recent Development of Small-Molecule Organic Fluorophores for Multifunctional Bioimaging in the Second near-Infrared Window. *J. Lumin.* 2020, 225, No. 117338.

(5) Madani, S. Y.; Shabani, F.; Dwek, M. V.; Seifalian, A. M. Conjugation of Quantum Dots on Carbon Nanotubes for Medical Diagnosis and Treatment. *Int. J. Nanomed.* 2013, 8, 941−950.

(6) Hong, G.; Antaris, A. L.; Dai, H. Near-Infrared Fluorophores for Biomedical Imaging. *Nat. Biomed. Eng.* 2017, 1, No. 0010.

(7) Li, C.; Chen, G.; Zhang, Y.; Wu, F.; Wang, Q. Advanced Fluorescence Imaging Technology in the Near-Infrared-II Window for Biomedical Applications. *J. Am. Chem. Soc.* 2020, 142, 14789−14804.

(8) Chen, C.; Tian, R.; Zeng, Y.; Chu, C.; Liu, G. Activatable Fluorescence Probes for "Turn-On" and Ratiometric Biosensing and Bioimaging: From NIR-I to NIR-II. *Bioconjugate Chem.* 2020, 31, 276−292.

(9) Heselich, A.; Frohns, F.; Frohns, A.; Naumann, S. C.; Layer, P. G. Near-Infrared Exposure Changes Cellular Responses to Ionizing Radiation. *Photochem. Photobiol.* 2012, 88, 135−146.

(10) Li, Q.; Ding, Q.; Li, Y.; Zeng, X.; Liu, Y.; Lu, S.; Zhou, H.; Wang, X.; Wu, J.; Meng, X.; Deng, Z.; Xiao, Y. Novel Small-Molecule Fluorophores for in Vivo NIR-IIa and NIR-IIb Imaging. *Chem. Commun.* 2020, 56, 3289−3292.

(11) Li, Y.; Liu, Y.; Li, Q.; Zeng, X.; Tian, T.; Zhou, W.; Cui, Y.; Wang, X.; Cheng, X.; Ding, Q.; Wang, X.; Wu, J.; Deng, H.; Li, Y.; Meng, X.; Deng, Z.; Hong, X.; Xiao, Y. Novel NIR-II Organic Fluorophores for Bioimaging beyond 1550 Nm. *Chem. Sci.* 2020, 11, 2621−2626.

(12) Fu, W.; Yan, C.; Guo, Z.; Zhang, J.; Zhang, H.; Tian, H.; Zhu, W.-H. Rational Design of Near-Infrared Aggregation-Induced-Emission-Active Probes: In Situ Mapping of Amyloid-β Plaques with Ultrasensitivity and High-Fidelity. *J. Am. Chem. Soc.* 2019, 141, 3171−3177.

(13) Vijayan, S. M.; Sparks, N.; Roy, J. K.; Smith, C.; Tate, C.; Hammer, N. I.; Leszczynski, J.; Watkins, D. L. Evaluating Donor Effects in Isoindigo-Based Small Molecular Fluorophores. *J. Phys. Chem. A* 2020, 124, 10777−10786.

(14) Goswami, S.; Gish, M. K.; Wang, J.; Winkel, R. W.; Papanikolas, J. M.; Schanze, K. S. π-Conjugated Organometallic Isoindigo Oligomer and Polymer Chromophores: Singlet and Triplet Excited State Dynamics and Application in Polymer Solar Cells. *ACS Appl. Mater. Interfaces* 2015, 7, 26828−26838.

(15) Sparks, N. E.; Dorris, A.; Vijayan, S. M.; Chandrasiri, I.; Zia, M. F.; Flynt, A.; Hammer, N. I.; Watkins, D. Effects of Nanoaggregation on Isoindigo-Based Fluorophores for near-Infrared Bioimaging Applications. *Mol. Syst. Des. Eng.* 2022, 7, 906−914.

(16) Tanaka, S.; Yamashita, Y. Synthesis of a Narrow Band Gap Heterocyclic Polymer: Poly-4,6-Di(2-Thienyl)Thieno[3,4-c][1,2,5]-Thiadiazole. *Synth. Met.* 1993, 55, 1251−1254.

(17) Bower, J. D.; Schlessinger, R. H. Synthesis of Two Nonclassical Thienothiadiazoles. *J. Am. Chem. Soc.* 1969, 91, 6891−6892.

(18) Steinberger, S.; Mishra, A.; Reinold, E.; Mena-Osteritz, E.; Müller, H.; Uhrich, C.; Pfeiffer, M.; Bäuerle, P. Synthesis and Characterizations of Red/near-IR Absorbing A−D−A−D−A-Type Oligothiophenes Containing Thienothiadiazole and Thienopyrazine Central Units. *J. Mater. Chem.* 2012, 22, 2701−2712.

(19) Ledwon, P. Recent Advances of Donor-Acceptor Type Carbazole-Based Molecules for Light Emitting Applications. *Org. Electron.* 2019, 75, No. 105422.

(20) Capodilupo, A. L.; Vergaro, V.; Baldassarre, F.; Cardone, A.; Corrente, G. A.; Carlucci, C.; Leporatti, S.; Papadia, P.; Gigli, G.; Ciccarella, G. Thiophene-Based Fluorescent Probes with Low Cytotoxicity and High Photostability for Lysosomes in Living Cells. *Biochim. Biophys. Acta, Gen. Subj.* 2015, 1850, 385−392.

(21) Leriche, P.; Frère, P.; Cravino, A.; Alévêque, O.; Roncali, J. Molecular Engineering of the Internal Charge Transfer in Thiophene−Triphenylamine Hybrid π-Conjugated Systems. *J. Org. Chem.* 2007, 72, 8332−8336.

(22) Li, Y.; Cai, Z.; Liu, S.; Zhang, H.; Wong, S. T. H.; Lam, J. W. Y.; Kwok, R. T. K.; Qian, J.; Tang, B. Z. Design of AIEgens for Near-Infrared IIb Imaging through Structural Modulation at Molecular and Morphological Levels. *Nat. Commun.* 2020, 11, No. 1255.

(23) Sun, P.; Chen, Y.; Sun, B.; Zhang, H.; Chen, K.; Miao, H.; Fan, Q.; Huang, W. Thienothiadiazole-Based NIR-II Dyes with D−A−D Structure for NIR-II Fluorescence Imaging Systems. *ACS Appl. Bio Mater.* 2021, 4, 4542−4548.

(24) Feng, Z.; Yu, X.; Jiang, M.; Zhu, L.; Zhang, Y.; Yang, W.; Xi, W.; Li, G.; Qian, J. Excretable IR-820 for *in Vivo* NIR-II Fluorescence Cerebrovascular Imaging and Photothermal Therapy of Subcutaneous Tumor. *Theranostics* 2019, 9, 5706−5719.

(25) Zarrintaj, P.; Ramsey, J. D.; Samadi, A.; Atoufi, Z.; Yazdi, M. K.; Ganjali, M. R.; Amirabad, L. M.; Zangene, E.; Farokhi, M.; Formela, K.; Saeb, M. R.; Mozafari, M.; Thomas, S. Poloxamer: A Versatile Tri-Block Copolymer for Biomedical Applications. *Acta Biomater.* 2020, 110, 37−67.

(26) Bora, C.; Dolui, S. K. Fabrication of Polypyrrole/Graphene Oxide Nanocomposites by Liquid/Liquid Interfacial Polymerization and Evaluation of Their Optical, Electrical and Electrochemical Properties. *Polymer* 2012, 53, 923−932.

(27) Bowkett, D.; Talon, R.; Tallant, C.; Schofield, C.; von Delft, F.; Knapp, S.; Bruton, G.; Brennan, P. E. Identifying Small-Molecule Binding Sites for Epigenetic Proteins at Domain−Domain Interfaces. *ChemMedChem* 2018, 13, 1051−1057.

(28) Chai, J.-D.; Head-Gordon, M. Long-Range Corrected Hybrid Density Functionals with Damped Atom−Atom Dispersion Corrections. *Phys. Chem. Chem. Phys.* 2008, 10, 6615−6620.

(29) Gaussian 09 Citation|Gaussian.com, 2023. https://gaussian.com/g09citation/. accessed March 08, 2023.

(30) Ding, F.; Zhan, Y.; Lu, X.; Sun, Y. Recent Advances in Near-Infrared II Fluorophores for Multifunctional Biomedical Imaging. *Chem. Sci.* 2018, 9, 4370−4380.

(31) Rathnamalala, C. S. L.; Hernandez, S.; Lucero, M. Y.; Swartchick, C. B.; Shaik, A. K.; Hammer, N. I.; East, A. K.; Gwaltney, S. R.; Chan, J.; Scott, C. N. Xanthene-Based Nitric Oxide-Responsive Nanosensor for Photoacoustic Imaging in the SWIR Window. *Angew. Chem., Int. Ed.* 2023, 62, No. e202214855.

(32) Wang, S.; Li, B.; Zhang, F. Molecular Fluorophores for Deep-Tissue Bioimaging. *ACS Cent. Sci.* 2020, 6, 1302−1316.

(33) Zhou, B.; Hu, Z.; Jiang, Y.; Zhong, C.; Sun, Z.; Sun, H. Theoretical Exploitation of Acceptors Based on Benzobis-(Thiadiazole) and Derivatives for Organic NIR-II Fluorophores. *Phys. Chem. Chem. Phys.* 2018, 20, 19759−19767.

(34) Hwang, Y.-J.; Kim, F. S.; Xin, H.; Jenekhe, S. A. New Thienothiadiazole-Based Conjugated Copolymers for Electronics and Optoelectronics. *Macromolecules* 2012, 45, 3732−3739.

(35) Bohra, H.; Tan, S. Y.; Shao, J.; Yang, C.; Efrem, A.; Zhao, Y.; Wang, M. Narrow Bandgap Thienothiadiazole-Based Conjugated Porous Polymers: From Facile Direct Arylation Polymerization to Tunable Porosities and Optoelectronic Properties. *Polym. Chem.* 2016, 7, 6413−6421.

(36) Thomas, A.; Ji, C.; Siddlingeshwar, B.; Manohar, P. U.; Ying, F.; Wu, W. Revealing the Biradicaloid Nature Inherited in the Derivatives of Thieno[3,4-c][1,2,5]Thiadiazole: A Computational Study. *Phys. Chem. Chem. Phys.* 2021, 23, 1050−1061.

(37) Kwon, O.; Barlow, S.; Odom, S. A.; Beverina, L.; Thompson, N. J.; Zojer, E.; Brédas, J.-L.; Marder, S. R. Aromatic Amines: A Comparison of Electron-Donor Strengths. *J. Phys. Chem. A* 2005, 109, 9346−9352.

(38) Staub, K.; Levina, G. A.; Barlow, S.; Kowalczyk, T. C.; Lackritz, H. S.; Barzoukas, M.; Fort, A.; Marder, S. R. Synthesis and Stability Studies of Conformationally Locked 4-(Diarylamino)Aryl- and 4-(Dialkylamino)Phenyl-Substituted Second-Order Nonlinear Optical Polyene Chromophores. *J. Mater. Chem.* 2003, 13, 825−833.

(39) Li, X.; Li, J.; Liu, D.; Li, D.; Dong, R. A Donor Design Strategy for Triazine-Carbazole Blue Thermally Activated Delayed Fluorescence Materials. *New J. Chem.* **2020**, *44*, 9743−9753.

(40) Tanaka, H.; Shizu, K.; Nakanotani, H.; Adachi, C. Twisted Intramolecular Charge Transfer State for Long-Wavelength Thermally Activated Delayed Fluorescence. *Chem. Mater.* **2013**, *25*, 3766−3771.

(41) Jeffries-EL, M.; Kobilka, B. M.; Hale, B. J. Optimizing the Performance of Conjugated Polymers in Organic Photovoltaic Cells by Traversing Group 16. *Macromolecules* **2014**, *47*, 7253−7271.

(42) Gershoni-Poranne, R.; Rahalkar, A. P.; Stanger, A. The Predictive Power of Aromaticity: Quantitative Correlation between Aromaticity and Ionization Potentials and HOMO−LUMO Gaps in Oligomers of Benzene, Pyrrole, Furan, and Thiophene. *Phys. Chem. Chem. Phys.* **2018**, *20*, 14808−14817.

(43) Cordell, F. R.; Boggs, J. E. Structure and Degree of Aromatic Character in Furan, Pyrrole, and Thiophene. *J. Mol. Struct.: THEOCHEM* **1981**, *85*, 163−178.

(44) Yang, Q.; Ma, Z.; Wang, H.; Zhou, B.; Zhu, S.; Zhong, Y.; Wang, J.; Wan, H.; Antaris, A.; Ma, R.; Zhang, X.; Yang, J.; Zhang, X.; Sun, H.; Liu, W.; Liang, Y.; Dai, H. Rational Design of Molecular Fluorophores for Biological Imaging in the NIR-II Window. *Adv. Mater.* **2017**, *29*, No. 1605497.

(45) Zhang, Y.; Autry, S. A.; McNamara, L. E.; Nguyen, S. T.; Le, N.; Brogdon, P.; Watkins, D. L.; Hammer, N. I.; Delcamp, J. H. Near-Infrared Fluorescent Thienothiadiazole Dyes with Large Stokes Shifts and High Photostability. *J. Org. Chem.* **2017**, *82*, 5597−5606.

(46) Brownell, L. V.; Robins, K. A.; Jeong, Y.; Lee, Y.; Lee, D.-C. Highly Systematic and Efficient HOMO−LUMO Energy Gap Control of Thiophene-Pyrazine-Acenes. *J. Phys. Chem. C* **2013**, *117*, 25236−25247.

(47) Wirz, J. Spectroscopic and Kinetic Investigations of Conjugated Biradical Intermediates. *Pure Appl. Chem.* **1984**, *56*, 1289−1300.

(48) Loos, P.-F.; Comin, M.; Blase, X.; Jacquemin, D. Reference Energies for Intramolecular Charge-Transfer Excitations. *J. Chem. Theory Comput.* **2021**, *17*, 3666−3686.

(49) McCormick, T. M.; Bridges, C. R.; Carrera, E. I.; DiCarmine, P. M.; Gibson, G. L.; Hollinger, J.; Kozycz, L. M.; Seferos, D. S. Conjugated Polymers: Evaluating DFT Methods for More Accurate Orbital Energy Modeling. *Macromolecules* **2013**, *46*, 3879−3886.

(50) Chandrasiri, I.; Yaddehige, M. L.; Li, B.; Sun, Y.; Meador, W. E.; Dorris, A.; Zia, M. F.; Hammer, N. I.; Flynt, A.; Delcamp, J. H.; Davis, E.; Lippert, A.; Watkins, D. L. Cross-Linking Poly-(Caprolactone)−Polyamidoamine Linear Dendritic Block Copolymers for Theranostic Nanomedicine. *ACS Appl. Polym. Mater.* **2022**, *4*, 2972−2986.

(51) Paramasivam, M.; Gupta, A.; Raynor, A. M.; Bhosale, S. V.; Bhanuprakash, K.; Rao, V. J. Small Band Gap D−π−A−π−D Benzothiadiazole Derivatives with Low-Lying HOMO Levels as Potential Donors for Applications in Organic Photovoltaics: A Combined Experimental and Theoretical Investigation. *RSC Adv.* **2014**, *4*, 35318−35331.

(52) Lei, Z.; Zhang, F. Molecular Engineering of NIR-II Fluorophores for Improved Biomedical Detection. *Angew. Chem., Int. Ed.* **2021**, *60*, 16294−16308.

(53) Yang, Q.; Hu, Z.; Zhu, S.; Ma, R.; Ma, H.; Ma, Z.; Wan, H.; Zhu, T.; Jiang, Z.; Liu, W.; Jiao, L.; Sun, H.; Liang, Y.; Dai, H. Donor Engineering for NIR-II Molecular Fluorophores with Enhanced Fluorescent Performance. *J. Am. Chem. Soc.* **2018**, *140*, 1715−1724.

(54) Yuen, J. D.; Wang, M.; Fan, J.; Sheberla, D.; Kemei, M.; Banerji, N.; Scarongella, M.; Valouch, S.; Pho, T.; Kumar, R.; Chesnut, E. C.; Bendikov, M.; Wudl, F. Importance of Unpaired Electrons in Organic Electronics. *J. Polym. Sci., Part A: Polym. Chem.* **2015**, *53*, 287−293.

(55) Rurack, K.; Rettig, W.; Resch-Genger, U. Unusually High Cation-Induced Fluorescence Enhancement of a Structurally Simple Intrinsic Fluoroionophore with a Donor−Acceptor−Donor Constitution. *Chem. Commun.* **2000**, *5*, 407−408.

(56) McNamara, L. E.; Rill, T. A.; Huckaba, A. J.; Ganeshraj, V.; Gayton, J.; Nelson, R. A.; Sharpe, E. A.; Dass, A.; Hammer, N. I.; Delcamp, J. H. Indolizine−Squaraines: NIR Fluorescent Materials with Molecularly Engineered Stokes Shifts. *Chem. - Eur. J.* **2017**, *23*, 12494−12501.

(57) Berezin, M. Y.; Akers, W. J.; Guo, K.; Fischer, G. M.; Daltrozzo, E.; Zumbusch, A.; Achilefu, S. Long Fluorescence Lifetime Molecular Probes Based on Near Infrared Pyrrolopyrrole Cyanine Fluorophores for In Vivo Imaging. *Biophys. J.* **2009**, *97*, L22−L24.

(58) Caspar, J. V.; Kober, E. M.; Sullivan, B. P.; Meyer, T. J. Application of the Energy Gap Law to the Decay of Charge-Transfer Excited States. *J. Am. Chem. Soc.* **1982**, *104*, 630−632.

(59) Ma, S.; Du, S.; Pan, G.; Dai, S.; Xu, B.; Tian, W. Organic Molecular Aggregates: From Aggregation Structure to Emission Property. *Aggregate* **2021**, *2*, No. e96.

(60) Witte, F.; Rietsch, P.; Sinha, S.; Krappe, A.; Joswig, J.-O.; Götze, J. P.; Nirmalananthan-Budau, N.; Resch-Genger, U.; Eigler, S.; Paulus, B. Fluorescence Quenching in J-Aggregates through the Formation of Unusual Metastable Dimers. *J. Phys. Chem. B* **2021**, *125*, 4438−4446.

(61) Sulas, D. B.; London, A. E.; Huang, L.; Xu, L.; Wu, Z.; Ng, T. N.; Wong, B. M.; Schlenker, C. W.; Azoulay, J. D.; Sfeir, M. Y. Preferential Charge Generation at Aggregate Sites in Narrow Band Gap Infrared Photoresponsive Polymer Semiconductors. *Adv. Opt. Mater.* **2018**, *6*, No. 1701138.

(62) Bhattacharjee, S. DLS and Zeta Potential − What They Are and What They Are Not? *J. Controlled Release* **2016**, *235*, 337−351.